Journal of Fluids and Structures (1997) **11,** 873–892

AERODYNAMICS AND DYNAMICS OF RECTANGULAR PRISMS WITH MOMENTUM INJECTION

S. R. Munshi and V. J. Modi

Department of Mechanical Engineering, The University of British Columbia Vancouver, B.C., Canada V6T 1Z4

and

T. Yokomizo

Department of Mechanical Engineering, Kanto Gakuin University Mutsuura, Kanazawa, Yokohama, Japan 236

(Received 19 February 1997 and in revised form 15 July 1997)

A structural member with rectangular cross-section is frequently encountered in civil, mechanical and ocean engineering applications. Structural loading in terms of steady and unsteady pressure fields, susceptibility to flow-induced instabilities, etc., for tall buildings, bridges, offshore platforms, marine risers and a wide variety of other configurations have been of interest to engineers. Recent progress in engineering materials and computer-aided design has led to structures with reduced stiffness, making them prone to wind, earthquake, as well as ocean-wave and current-excited oscillations. The present research is aimed at understanding these issues at a fundamental level through a comprehensive study of moving-surface boundary-layer control (MSBC) as applied to two-dimensional rectangular prisms with reference to drag reduction and suppression of flow-induced vibrations. Extensive wind-tunnel tests, complemented by quasisteady analysis and flow visualization study, suggest that the concept of MSBC represents a versatile tool for drag reduction and suppression of both vortex resonance and galloping type of instabilities.

1. INTRODUCTION

The dynamic character of the flow field around a bluff body generally manifests in the form of flow stagnation in the front, shear layer separation and reattachment on the sides, as well as a turbulent-vortex wake downstream over a wide range of Reynolds numbers ($1 < \mathrm{Re} < 10^7$). In contrast to streamlined objects, a bluff body has almost no pressure recovery region on the rear half of the body, resulting in a high drag. Literature pertaining to bluff-body wakes and vortex shedding has been reviewed by Rosenhead (1990), Bearman (1967), Mair & Maull (1971); Berger & Wille (1972), Hussaini & Salas (1987), Roshko (1993), Williamson (1996), and others.

1.1. Vortex Resonance and Galloping Type of Instabilities

For a flexibly mounted bluff body, transverse vibrations known as vortex resonance could occur if the vortex-shedding frequency (f_v) and the structural natural frequency (f_n) are close to each other. A structure could also experience galloping, which is a form of

0889–9746/97/080873 + 20 $25.00/fl970108

self-excited vibrations, where the body generates an aerodynamic force aiding the motion, which could build up into large amplitude, low-frequency vibrations. Sometimes such vibrations could have catastrophic consequences. The Tacoma Narrows Bridge disaster in 1940, in the U.S.A., is all too well known.

Vertex resonance and galloping types of vibrations have regularly been reported for tall buildings, suspension bridges, smokestacks, bundles of tubes in nuclear reactors, submarine periscopes, ice-covered transmission lines, offshore platforms and similar bluff bodies. A vast body of literature accumulated over the years has been reviewed by several authors, including Marris (1964), Bearman (1984), Parkinson (1989) and others.

1.2. Control of Flow-Induced Instabilities

Recent advances in computer-aided engineering and material science have led to structures with reduced mass and stiffness, making them prone to wind, earthquake, as well as ocean-wave and current-excited oscillations. The 21st century would witness super-tall buildings (>1000 m) and extra-long span bridges (>2000 m) with pylons as high as 300 m, as pointed out by Kubo *et al.* (1994). The conventional approach to vibration control is through increased structural damping using tuned mass or mutation dampers. Zdravkovich (1981) and Modi *et al.* (1995) have reviewed the literature pertaining to various devices employed for vibration control of structures. Anywhere from 0·5 to 3% of the weight of the structures is necessary for such devices to be effective. Of course, there is a limit as to how large a weight could be acceptable as the structure grows taller. The alternative approach to vibration suppression would be to modify the forces responsible for the vibrations. One way to achieve this would be to prevent, or at least delay, separation of the boundary layer from the wall of the structure. A moving wall contributes to this objective in several ways: (a) it retards the growth of the boundary layer by minimizing the relative motion between the surface and the free stream; (b) it injects momentum into the boundary layer; (c) it creates a region of high suction and thereby accelerates the flow in its neighbourhood outside of the boundary layer; and (d) it delays separation and interferes with the evolution of the wake.

Using rotating cylinders as momentum injecting elements, wind tunnel tests with a family of aerofoils have shown moving-surface boundary-layer control (MSBC) to be remarkably successful in delaying separation of the boundary layer (Modi *et al.* 1991). Munshi *et al.* (1995) have reported successful drag reduction and vibration control of a two-dimensional D-section geometry. Kubo *et al.* (1994) applied the concept of MSBC to the control of vortex resonance and galloping type of instabilities associated with a two-dimensional square prism.

1.3. Flow past Rectangular Prisms

In a study of two-dimensional (2-D) rectangular cylinders ($0 < \mathrm{AR} \leq 5$), Norberg (1993) detected the presence of multiple-vortex-shedding frequencies at small angles of attack. For rectangular prisms, a plot of the drag coefficient against the aspect ratio clearly shows that the C_D peaks between $0{\cdot}6 < \mathrm{AR} < 0{\cdot}7$ (Hamel-Derouich 1991). This can be explained in terms of a smaller wake cavity leading to an increase in the base suction. For $\mathrm{AR} > 0{\cdot}7$, the vortices are forced to form further dowmstream, because of the influence of the trailing-edge corners, resulting in a lower drag. Nakamura *et al.* (1991) have reported galloping of rectangular cylinders ($\mathrm{AR} \leq 5$) even in the presence of a splitter plate.

Experiments on a blunt flat plate and rectangular cylinders by Li & Melbourne (1995) suggest that it is necessary to correctly model both the turbulence intensity and scale to predict the peak design pressure loading on a structure. An increase in turbulence scale caused higher spanwise correlation of the flow field. Nakamura (1993) has carried out extensive study of the interactions between the turbulence and various 2-D and 3-D bluff rectangular cylinders. The results identify two distinct turbulence length scales (L_x) associated with the bluff-body flows: (i) shear-layer thickness scale, $L_x/D \sim 0{\cdot}1$ and (ii) body-scale turbulence, $L_x/D \sim 1{\cdot}0$. For $L_x/D > 2$–3, the effect of turbulence scale on the bluff-body flow becomes negligible. Nakamura's results also suggest that shear-layer-scale turbulence causes earlier reattachment of the flow through enhanced mixing, making a system with hard galloping characteristics soft, and the soft galloping even weaker.

With this as background, the present study focuses on the following.

(i) Extensive wind tunnel tests with a static, two-dimensional model of the rectangular prism (Figure 1, AR = 0·5, 2) to assess its aerodynamics as affected by the momentum injection and the angle of attack. The results show the MSBC to be effective in delaying the boundary-layer separation and vortex shedding, resulting in a significant drag reduction.

(ii) Investigation of two distinct forms of flow-induced vibrations using a specially designed dynamic test rig. The results suggest the MSBC to be quite successful in suppressing both vortex resonance and galloping type of instabilities. The wind-tunnel results agree well with the theoretical predictions based on quasisteady analysis.

(iii) An extensive flow visualization study in a closed-circuit water channel using slit lighting in conjunction with polyvinyl chloride tracer particles. It shows, rather dramatically, the effectiveness of MSBC as applied to a rectangular prism.

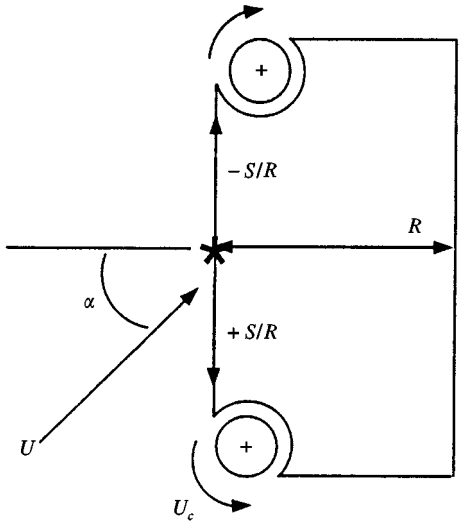

Figure 1. Geometry of the rectangular prism with rotating elements.

2. WIND-TUNNEL TEST RESULTS AND DISCUSSION

2.1. Model and Test Arrangement

The experiments were carried out in the closed-circuit, low-turbulence wind tunnel, where the air speed can be varied in the range of 1–40 m/s with a turbulence level less than 0·1%. A rectangular prism model, fitted with rotating cylinders, spanned the tunnel test section, $0{\cdot}91 \times 0{\cdot}68$ m, to create an essentially two-dimensional condition. The spatial variation of velocity in the tunnel test section is less than 0·25%.

The smooth surface rotating cylinders were mounted between high-speed self-aligning bearings housed in the brackets at either end of the model. They were driven by 0·25 h.p. variable speed a.c. motors, located outside the tunnel, through standard couplings. The model was provided with 30 pressure taps, suitably distributed over the circumference, to yield detailed information concerning the surface loading. The pressure distribution was recorded using a 48-channel scanivalve pressure transducer, with an accuracy of $2{\cdot}54 \times 10^{-3}$ mV/N/m^2, connected to a computerized data-acquisition system. The pressure data were recorded over 5 s with a sampling rate of 100 Hz. The mean static pressure was obtained through the arithmetic average over the sample. The pressure conveying tube (inner diameter, 1·67 mm) had little effect on attenuation and the phase response of the signal. The aerodynamic force data were obtained through integration of the pressure distribution.

The tests were conducted over a complete range of the angle of attack ($\alpha = 0$–180°) with an increment anywhere from 5° to 30° depending on the flow-field of interest. The cylinder rotation speed was varied to give U_c/U (U = free-stream wind speed, U_c = cylinder surface speed) in the range 0–4 with the Reynolds number of around 52 000 (based on the free-stream velocity and width of the flat face of the rectangular prism normal to the flow).

A remark concerning measurement of the pressure at the rotating cylinder would be appropriate. This information is crucial, since it represents a high suction region. Of course, monitoring of pressure at the surface of the rectangular prism is rather routine; however, the corresponding measurements at the surface of the cylinder typically rotating at 6000–12 000 r.p.m. presents a challenge. The problem was resolved by measuring the pressure in the vicinity of the cylinder rather than on the surface itself. This was achieved by keeping the pressure taps stationary while the cylinder rotated. By locating the tap in a narrow ring, the width of which represented only a very small fraction of that of the cylinder, it was possible to ensure continuity of the flow over the entire surface and to obtain an estimate of the surrounding pressure. The cylinder was provided with grooves to house the "pressure rings' while maintaining the cylinder surface uniform. Figure 2 shows details of the geometry and position of the pressure taps.

The relatively large angles of attack used in the experiments result in a considerable blockage of the wind-tunnel test section, from 15% at $\alpha = 0$ to 17% at $\alpha = 30^\circ$. The wall confinement leads to an increase in local wind speed at the location of the model, thus resulting in an increase in aerodynamic forces. Several approximate correction procedures have been reported in the literature to account for this effect. However, these procedures are mostly applicable to streamlined bodies with attached flow. A satisfactory procedure applicable to a bluff body offering a large blockage in a flow with separating shear layers is still not available.

With rotation of the cylinder(s), the problem is further complicated. As shown by the pressure data and confirmed by flow visualization, the unsteady flow can be separating and reattaching over a large portion of the top surface. In the absence of any reliable procedure

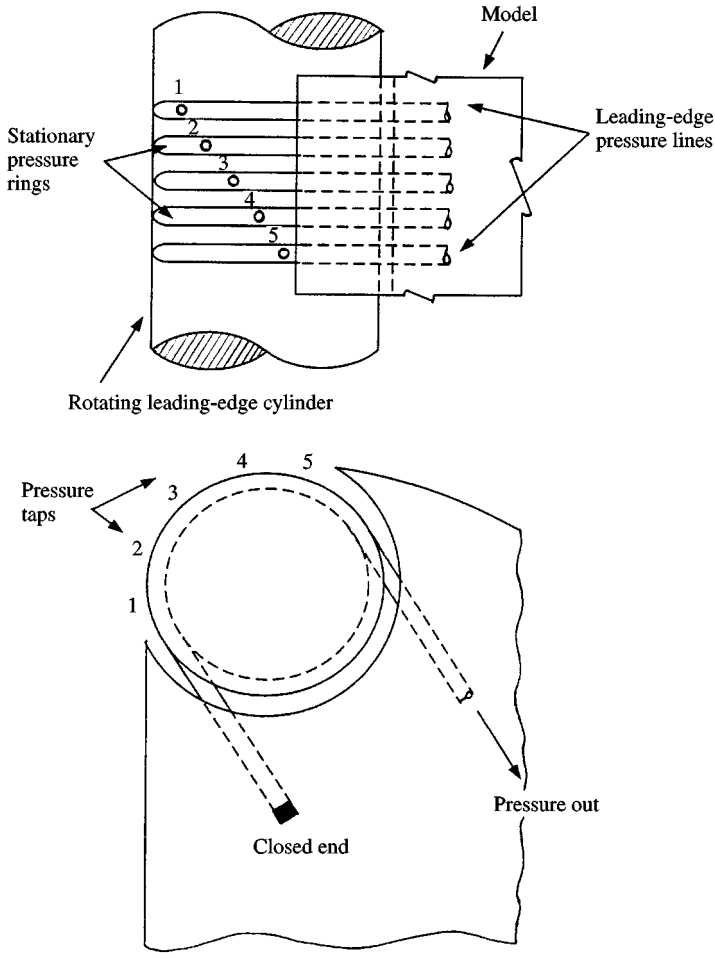

Figure 2. Schematic diagram showing details of the pressure taps near the rotating elements.

to account for wall confinement effects in the present situation, the results are purposely presented in uncorrected form. This does not detract from the main objective, as the blockage remains the same without and with the MSBC.

2.2. Mean Pressure Distribution

Figure 3(a–c) shows the pressure distribution at various angles of attack (α) with cylinders stationary ($U_c/U = 0$) as well as rotating ($U_c/U = 2, 4$). At $\alpha = 0$, essentially the entire front face of the rectangular prism (AR = 0·5) is a stagnation zone, and the overall pressure distribution is symmetric about the stagnation point. The fluid accelerates around the rounded corners resulting in large suction peaks located on the surface of the rotating cylinder. In the absence of momentum injection, the boundary layer separates near the corners as it encounters adverse pressure gradients, and the rest of the afterbody lies in the wake. As the momentum injection is increased from $U_c/U = 0 \rightarrow 4$, the pressure distribution

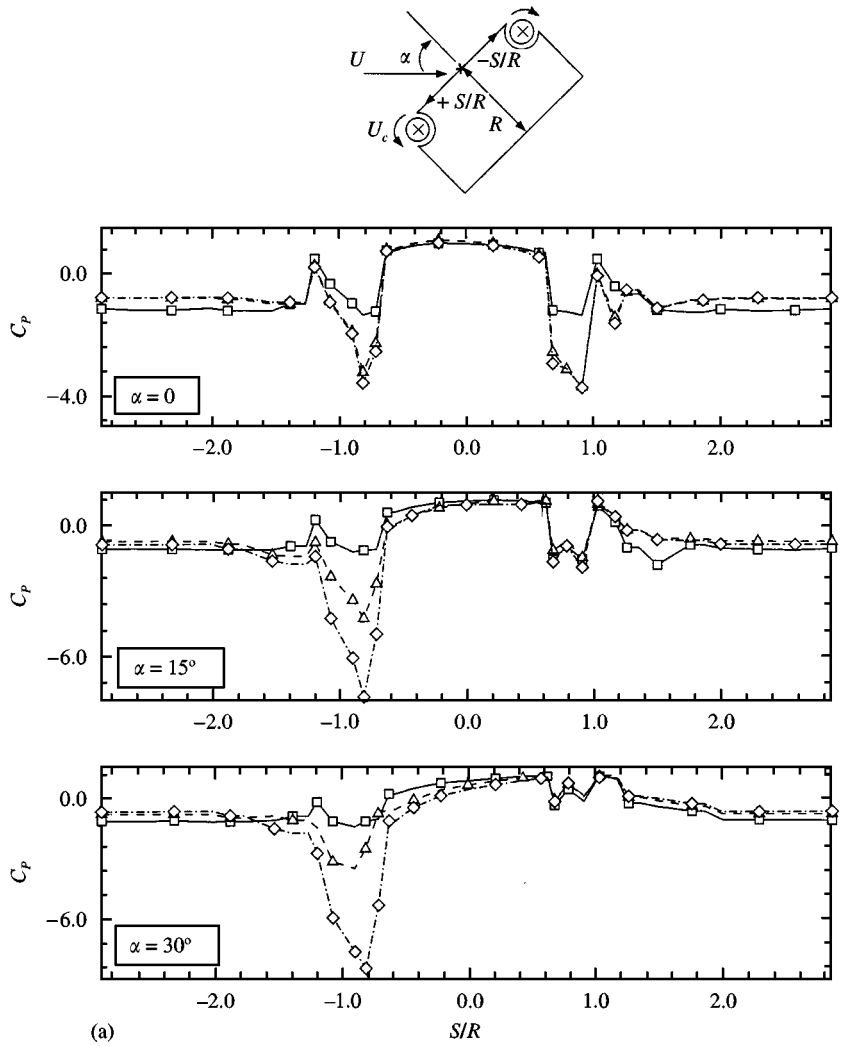

Figure 3(a). Surface pressure plots for the rectangular prism showing effects of the angle of attack and momentum injection: $\alpha = 0$, 15°, 30°; Re = 52 000. –□–, $U_c/U = 0$; – –Δ– –, $U_c/U = 2$; –·–◇–·–, $U_c/U = 4$.

is altered substantially. A marked increase can be observed in the suction peaks, which grows with an increase in the rate of momentum injection. In the presence of momentum injection, the separating shear layers are brought closer to the side faces of the rectangular prism, resulting in a smaller cavity in the near-wake region, and consequently, a higher base pressure and a lower drag. This decrease in the wake pressure is directly related to an increased curvature of the streamlines (Hamel-Derouich 1991).

As the angle of attack is increased from zero, the symmetry in the pressure distribution is no longer present. The stagnation point starts moving towards the lower rotating cylinder which is upstream of the second rotating element (i.e., the upper cylinder). The suction peaks on the rotating cylinders are no longer of equal strength: the one on the upstream rotating

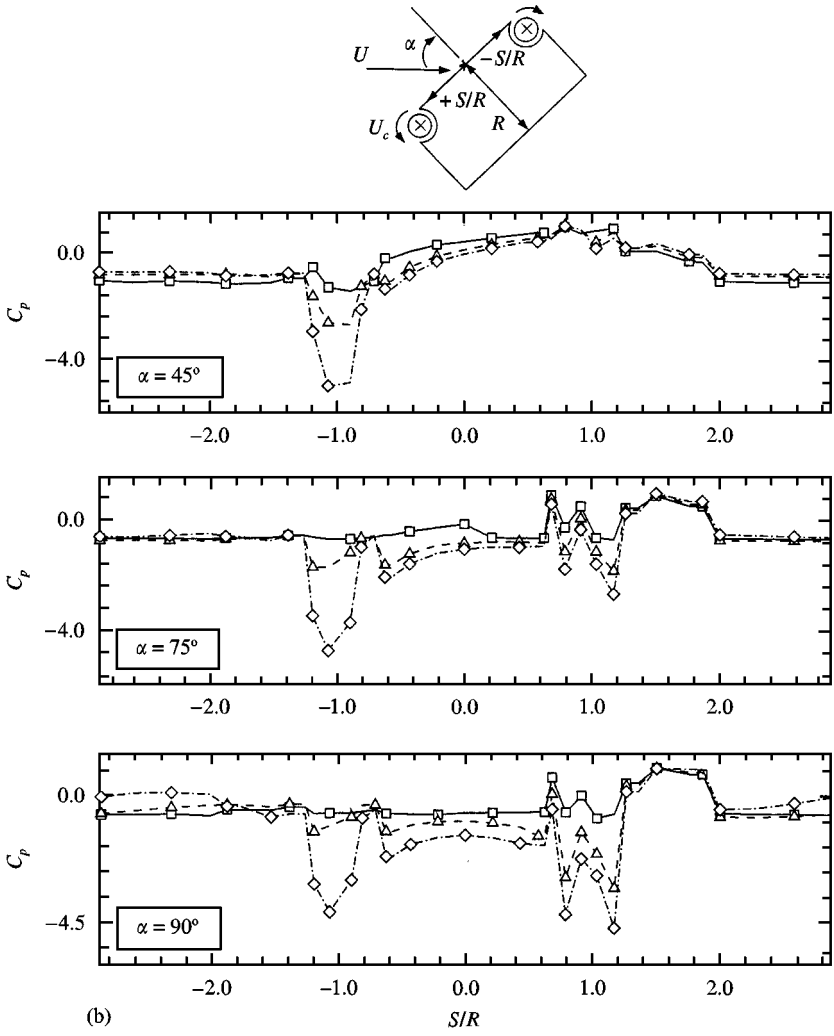

Figure 3(b). Surface pressure plots for the rectangular prism showing effects of the angle of attack and momentum injection: $\alpha = 45°$, 75°, 90°; Re = 52 000. –□–, $U_c/U = 0$; – – Δ – –, $U_c/U = 2$; –·–◇–·–, $U_c/U = 4$.

cylinder is weaker, while the downstream suction peak becomes more pronounced ($0 \leq \alpha \leq 45°$). At $\alpha = 15$–$20°$, there are two small stagnation zones on either side of the rotating cylinder. For $\alpha \geq 20°$, the stagnation point moves very close to the upstream rotating cylinder and merges with the suction peak. This causes the upstream suction peak to disappear even at the highest rate of momentum injection ($U_c/U = 4$). Thus, the movement of the stagnation point has an important influence on the overall pressure distribution. At $\alpha = 90$–$105°$, the suction peak reappears on the upstream rotating cylinder. For $\alpha \geq 135°$, almost the entire body lies in the wake. Now the rotation of cylinders, in the directions shown, does not make any difference. For $\alpha \geq 135°$ it would be necessary to reverse the direction of both rotating cylinders.

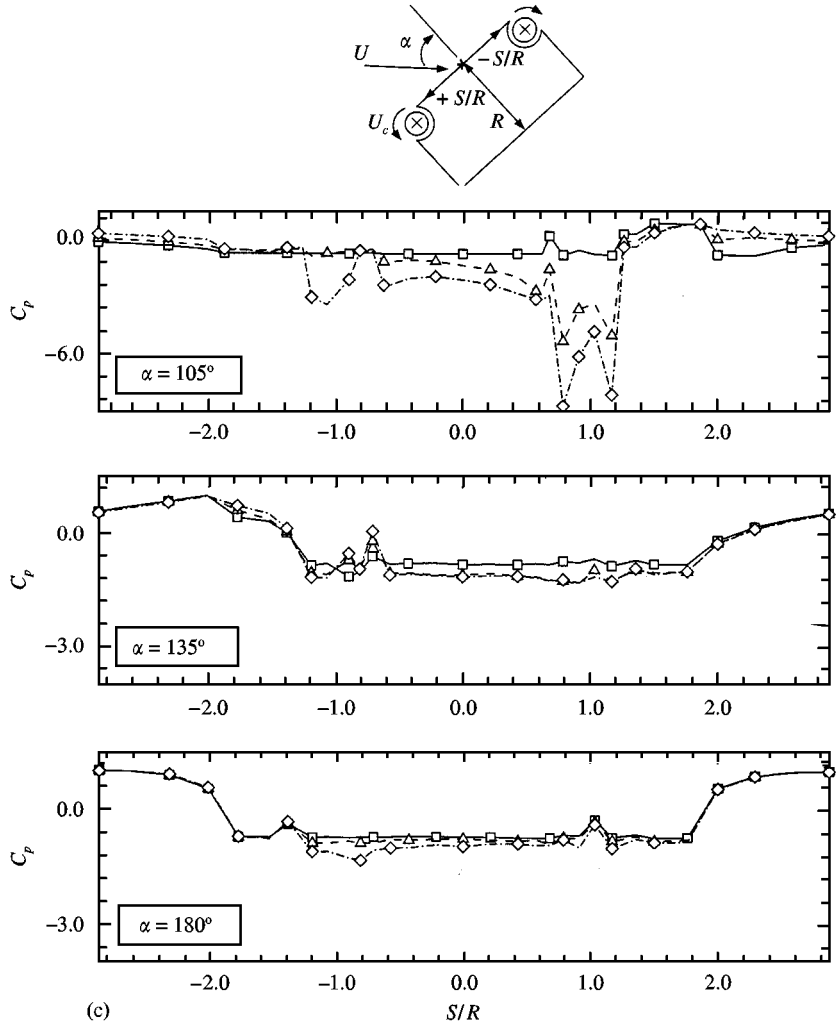

Figure 3(c). Surface pressure plots for the rectangular prism showing effects of the angle of attack and momentum injection: $\alpha = 105°, 135°, 180°$; Re = 52 000. –□–, $U_c/U = 0$; – – Δ – –, $U_c/U = 2$; –·–◇–·–, $U_c/U = 4$.

2.3. Aerodynamic Forces

The behaviour of the drag (C_D) and lift (C_L) coefficients (based on the frontal height of the rectangular prism) with the angle of attack (α) is presented in Figure 4. It is clearly shown that a substantial drag reduction takes place in the presence of MSBC. At $\alpha = 0$, a reduction in drag by 61% is indeed remarkable. An average of 36% drag reduction was achieved in the range $0 \leq \alpha \leq 75°$. For $90° \leq \alpha \leq 135°$, the effect of momentum injection is adverse, since the direction of the upstream cylinder is not correct. Reversing the direction of the upstream cylinder significantly lowers the drag coefficient. For $\alpha \geq 135°$, the inward mode of momentum injection (i.e. reversal in the direction of both upstream and downstream rotating cylinders) is necessary to achieve drag reduction.

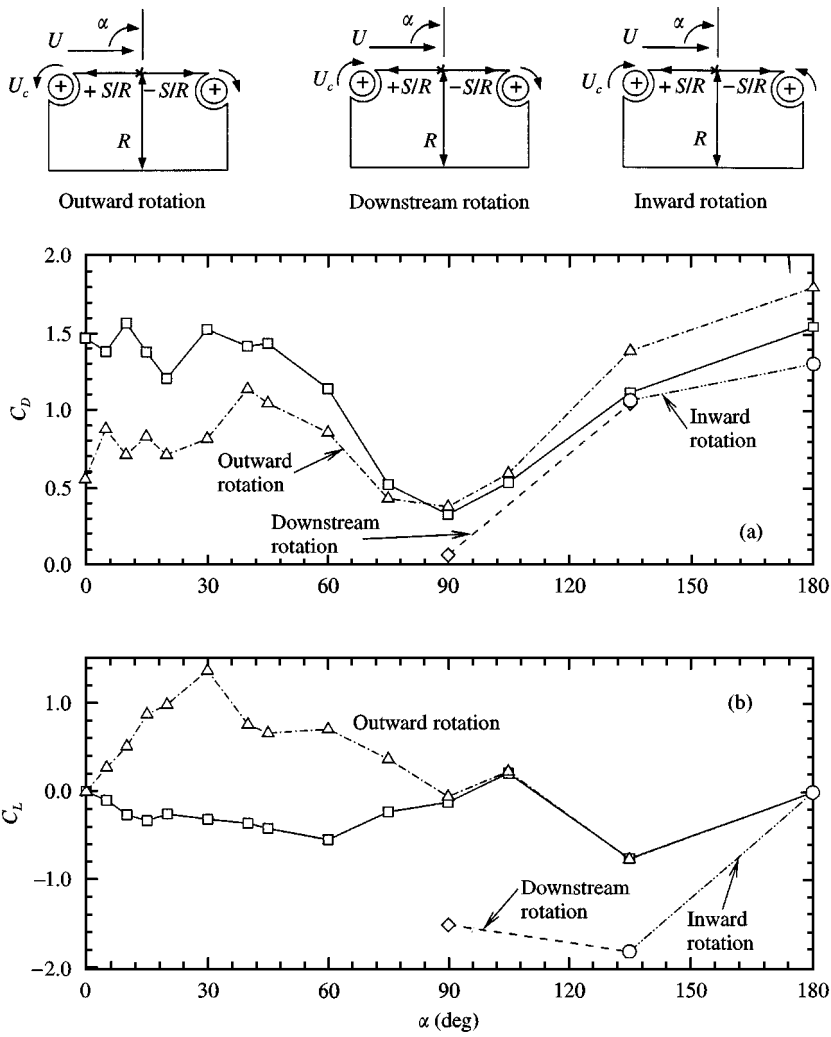

Figure 4. Drag and lift characteristics of the rectangular prism as affected by the momentum injection; Re = 52 000: –□–, $U_c/U = 0$; –·–Δ–·–, – –◇– –, – – ·· –○– ·· – –, $U_c/U = 4$.

For $\alpha = 0$ and 180°, the rectangular prism is symmetric with respect to the flow direction and the lift coefficient is zero. However, for $0 \leq \alpha \leq 75°$, a large increase in the lift coefficient is observed as the momentum injection is increased to $U_c/U = 4$. A negative $dC_L/d\alpha$ for $U_c/U = 0$ indicates a likelihood of galloping type of instability (Den Hartog 1956). In the presence of MSBC ($U_c/U = 4$) the slope becomes positive, which suggests stability.

It is expected that the benefit in terms of drag reduction cannot continue indefinitely as the momentum injection keeps increasing. At some critical value (U_{cr}/U) the drag reduction would level off. Figure 5 shows the C_D versus U_c/U curve for $\alpha = 0°$, 20° and 75°. It is obvious that the critical rate of momentum injection is ≈ 3.

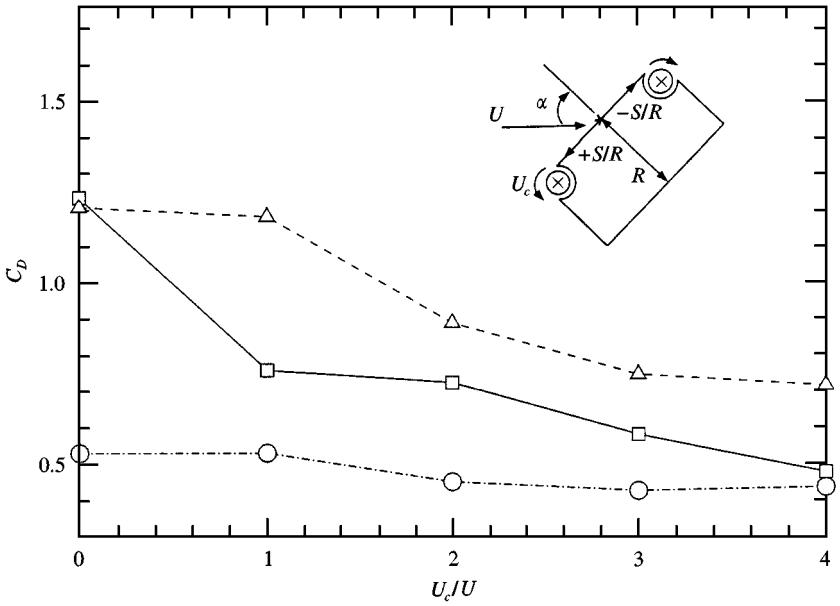

Figure 5. Effectiveness of increasing the momentum injection on the drag of a rectangular prism; Re = 52 000: –□–, $\alpha = 0$; – –Δ– –, $\alpha = 20°$; –·–○–·–, $\alpha = 75°$.

2.4. Base Pressure, Strouhal Number and Suppression of Vortex Shedding

The dependence of the base pressure on the angle of attack and rate of momentum injection is shown in Figure 6(a). Pressure tap A was used for the purpose of base-pressure measurement, as it always remains in the wake for $0 \leq \alpha \leq 105°$. For $\alpha > 105°$, tap B was used for the purpose. In general, the base-pressure coefficient is much lower than the free-stream value ($C_{Pb} < 0$), and increases significantly in presence of the MSBC. The average rise in the base pressure was around 24% for $0 \leq \alpha \leq 75°$. Figure 6(b) shows variation in the Strouhal number (St) with α. At $\alpha = 90°$ there is a sudden jump in the vortex-shedding frequency, indicating a favourable orientation of the rectangular prism. Now it acts like a streamlined geometry. A small but consistent rise in the Strouhal number is observed in the presence of MSBC ($U_c/U = 1$). At $U_c/U = 2$, no vortex shedding could be detected. A comparison with the experiment by Roshko (1955) involving a splitter plate behind a circular cylinder is relevant here. In the case of a splitter plate close to the cylinder, there is a rise in the base pressure, coupled with a decrease in the Strouhal number. On the other hand, in the presence of MSBC the rise in the base pressure is associated with a higher Strouhal number due to an increased streamlining of the bluff rectangular prism. Thus, there is a fundamental difference in these two mechanisms, though the end result is the same, i.e. the suppression of vortex shedding and drag reduction.

The vortex-shedding frequency and the base pressure are functions of the angle of attack. Hence, it would be logical to look for a universal parameter which can be used to compare the wakes of different bluff bodies, or a single bluff body at different orientations. Furthermore, it would be interesting to assess the effect of momentum injection on such a parameter. Attempts in this direction were made by Roshko (1955), Bearman (1967) and others.

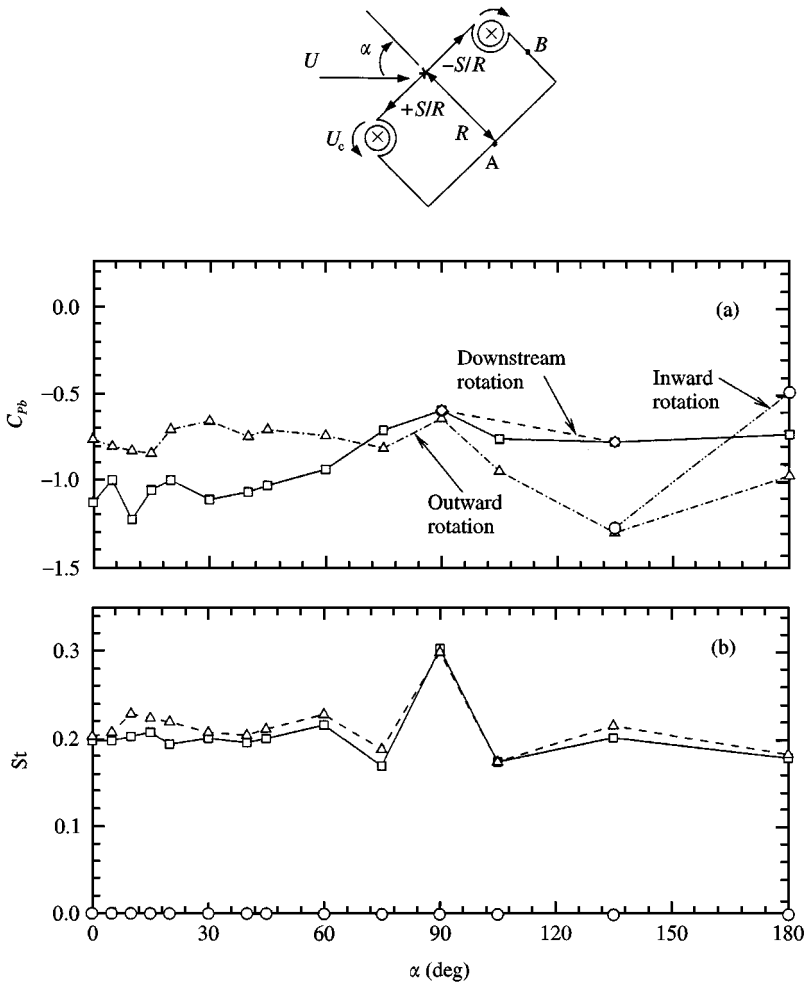

Figure 6. Effect of momentum injection on the wake pressure and Strouhal number of the rectangular prism; Re = 52 000: –□–, $U_c/U = 0$. (a) –·–Δ–·–, – –◇– –, – –·–○–·–, $U_c/U = 4$. (b) – –Δ– –, $U_c/U = 1$; o, $U_c/U = 2$.

The Strouhal number based on the projected height (h) is defined as

$$\mathrm{St}_p = \frac{f_v h}{U}, \tag{1}$$

while the universal Strouhal number (Su) is the ratio of St_p and the base-pressure parameter k_1,

$$\mathrm{Su} = f_v h/U k_1 = \mathrm{St}_p/k_1, \tag{2}$$

where $k_1 = \sqrt{1 - C_{Pb}}$. For a given bluff body, the quantities f_v, h, and k_1 are all functions of α; hence, at a given fluid velocity (U),

$$\mathrm{Su} = F(\alpha)/G(\alpha). \tag{3}$$

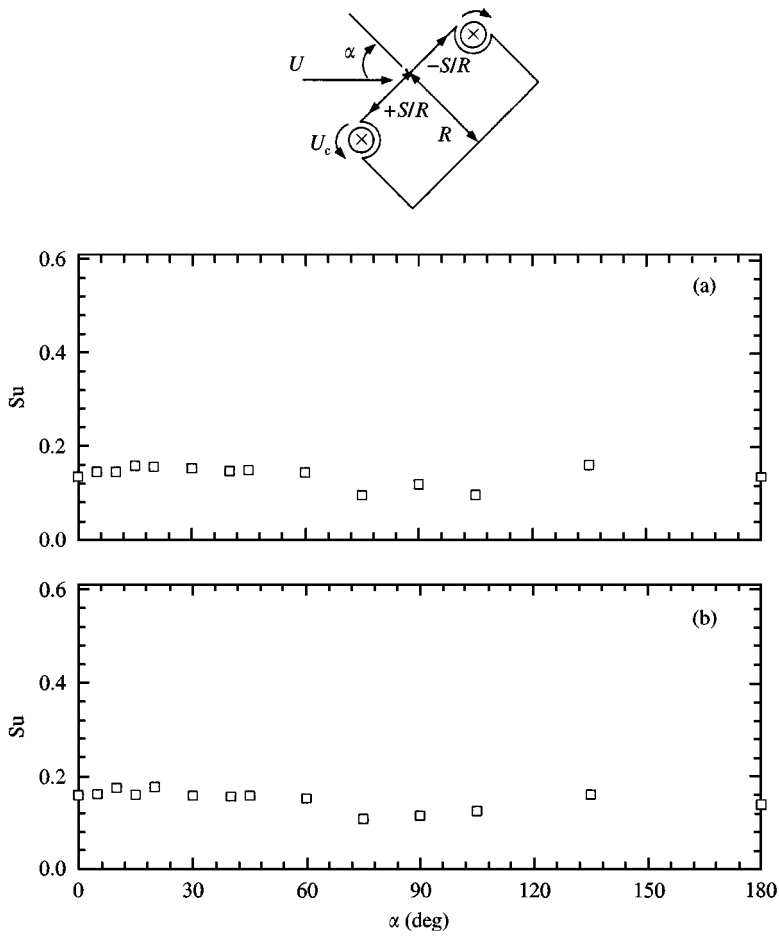

Figure 7. Effect of the angle of attack on the universal Strouhal number Su: (a) no momentum injection, $U_c/U = 0$; (b) with momentum injection, $U_c/U = 4$; Re = 52 000.

Figure 7 shows the relative insensitivity of Su with α both in the absence and presence of momentum injection. At $U_c/U = 1$, the mean value of Su is higher (0·15) as compared to 0·14 at $U_c/U = 0$. This correlation between St_p and k_1 confirms the observation made by Roshko (1955) that the wakes of various bluff bodies are similar, except the changes in geometric and velocity scales.

By performing power-spectrum analysis of the pressure versus time signals, a spectrum of frequencies is obtained with a dominant peak at the vortex-shedding frequency. In the absence of MSBC, a peak at the vortex-shedding frequency is clearly visible [Figure 8(a)], which is completely eliminated by a small amount of momentum injection [Figure 8(b)]. A flow visualization study reported later confirmed this physical character of the flow.

2.5. Theoretical Prediction of Galloping Instability

The governing equation of motion describing flow-induced vibration is generally non-linear in character, and hence difficult to solve. In the quasisteady theory proposed to study

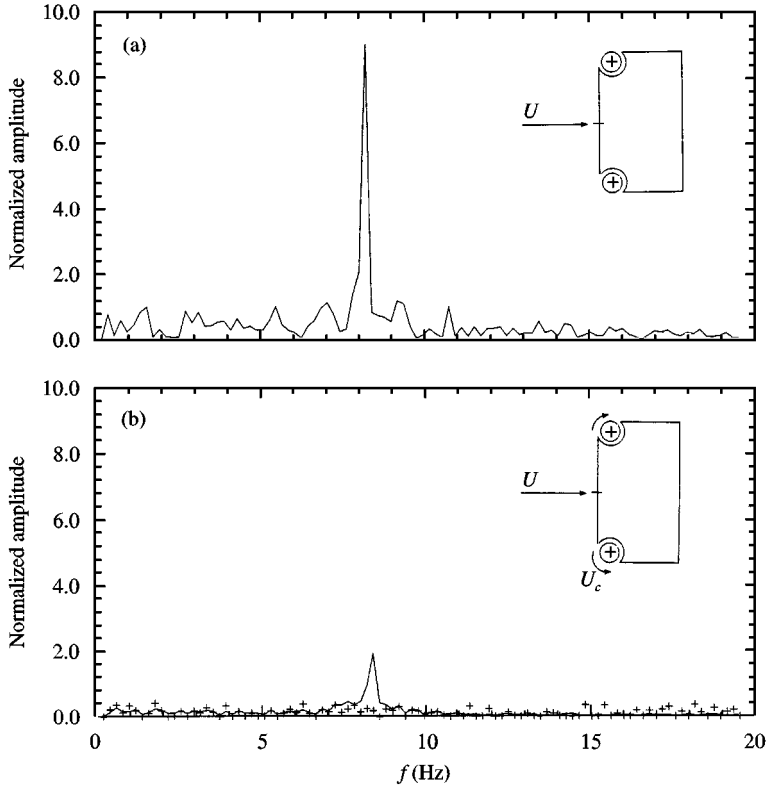

Figure 8. Power spectral representation of the wake pressure showing reduction in the strength of the shed vortex in the presence of the momentum injection: (a) $U_c/U = 0$; (b) with momentum injection: —, $U_c/U = 1$; +, $U_c/U = 2$.

galloping motion (Parkinson & Brooks 1961), the excitation force is approximated through a non-linear negative damping term in the equation of motion. The theory assumes that the bluff body, at any instant during the galloping cycle, experiences the same lateral force as that when held stationary at the same angle of attack $[\alpha = \tan^{-1}(\dot{y}/U)]$. The governing equation of motion as given by Parkinson & Brooks (1961) is

$$m\ddot{y} + r\dot{y} + ky = \tfrac{1}{2}\rho U^2 C_y D l_1, \tag{4}$$

with

$$C_y(\alpha) = P_1\left(\frac{\dot{y}}{U}\right) - P_3\left(\frac{\dot{y}}{U}\right)^3 + P_5\left(\frac{\dot{y}}{U}\right)^5 - P_7\left(\frac{\dot{y}}{U}\right)^7, \tag{5}$$

and P_i ($i = 1, 3, 5, 7$) are the coefficients of the polynomial expansion. They can be obtained from the curve of C_y against α using the least-squares technique. As a first approximation, neglecting higher-order terms, the total damping becomes

$$\frac{rnP_1}{2\beta}\left(\frac{2\beta}{nP_1} - V\right). \tag{6}$$

Here the term β represents the internal damping of the structure, which remains constant. As long as the fluid velocity $V < 2\beta/(nP_1)$, there is a net positive damping, i.e. dissipation of energy. At some critical velocity, $V_c = 2\beta/(nP_1)$, the total damping is zero and beyond that the damping becomes negative, leading to the galloping instability.

The lateral force coefficient can be defined in terms of the aerodynamic coefficients as

$$C_y = -(C_L + C_D \tan\alpha)\sec\alpha, \tag{7}$$

and the criterion for galloping instability becomes $\mathrm{d}C_y/\mathrm{d}\alpha > 0$ (Parkinson & Brooks 1961) for small α. If the integral, $I = 2\int_0^{y_m} F_y \,\mathrm{d}y$, (where $\pm y_m$ is the maximum amplitude); i.e. the work done over a cycle is positive, and energy could build up in the system. Such a situation is likely to occur in the case of a steady fluid flow past an unstable structure. The resultant oscillatory motion has a character of a limit cycle in the phase plane $(y, \dot{y})$. The higher-order terms in equation (5) eventually limit the amplitude of vibration.

The force results for the rectangular prism are shown in Figure 9. For $0 < \alpha < 15^\circ$, the system remains stable $(\mathrm{d}C_y/\mathrm{d}\alpha = 0)$ in the absence of momentum injection. For $15^\circ \leq \alpha \leq 45^\circ$, $\mathrm{d}C_y/\mathrm{d}\alpha < 0$, and the rectangular prism is stable. In the presence of

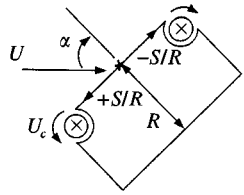

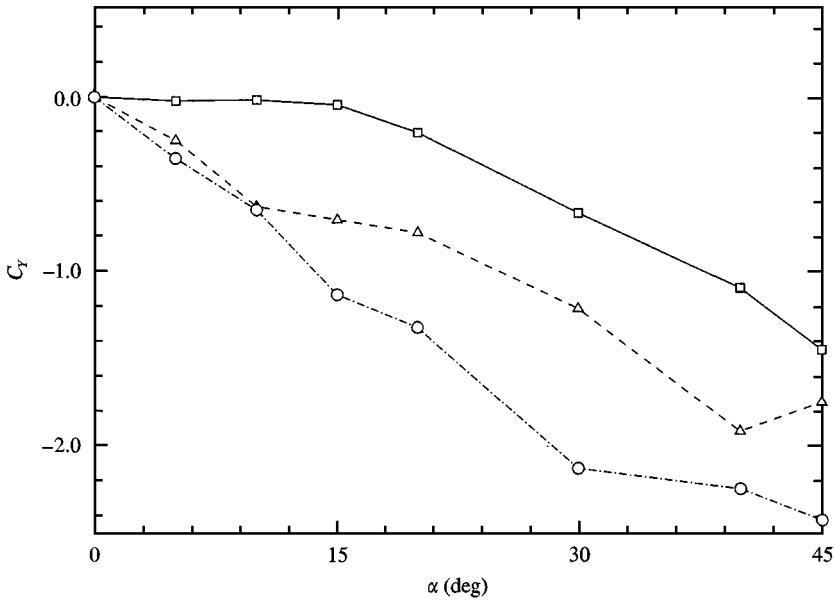

Figure 9. The rectangular prism is neutrally stable $(\mathrm{d}C_y/\mathrm{d}\alpha = 0)$ for $\alpha \leq 20^\circ$ in the absence of momentum injection $(U_c/U = 0)$. The stability is significantly improved $(\mathrm{d}C_y/\mathrm{d}\alpha < 0)$ with the cylinder rotation $(U_c/U = 2, 4)$; Re = 52 000. –□–, $U_c/U = 0$; – –Δ– –, $U_c/U = 2$; –·–○–·–, $U_c/U = 4$.

momentum injection ($U_c/U = 4$), $dC_y/d\alpha$ becomes -4.1 ($\alpha \leq 30^\circ$) and the stability is improved significantly. The presence of rotating cylinders has the effect of rounding the corners of the rectangular prism. Parkinson & Brooks (1961) have reported the stability study of a rectangular prism (AR = 0·5) with sharp corners.

2.6. Suppression of Vortex Resonance and Galloping Instability

Though the stationary-model wind-tunnel data provide sufficient information to predict the possible susceptibility of a structure to vortex resonance and galloping instabilities, it was considered appropriate to confirm the predictions through experiments. The experiments were conducted using a specially designed dynamic test rig which held a set of four air bearings for the model support, a displacement transducer, as well as controlled eddy current damper and springs to impart desired stiffness to the model (Figure 10). A light-weight balsa wood model, fitted with momentum injection rotating elements, was free to vibrate transversely to the flow direction. A real-time spectrum analyser and computer-based data-acquisition system were used to identify vortex resonance and galloping instabilities.

Figure 11 shows the amplitude response of the rectangular prism at $\alpha = 0$ as affected by the momentum injection. In the absence of momentum injection, as the wind speed is increased from zero, the rectangular prism experiences vortex resonance in the range $0{\cdot}9 \leq V \leq 1{\cdot}3$. This finite band of velocities indicates the entrainment of the vortex-shedding frequency by the system natural frequency. For $V > 1{\cdot}3$, the rectangular prism becomes stable as the vortex-shedding frequency is now higher than the system natural frequency. With a further increase in the wind velocity, there is no onset of galloping

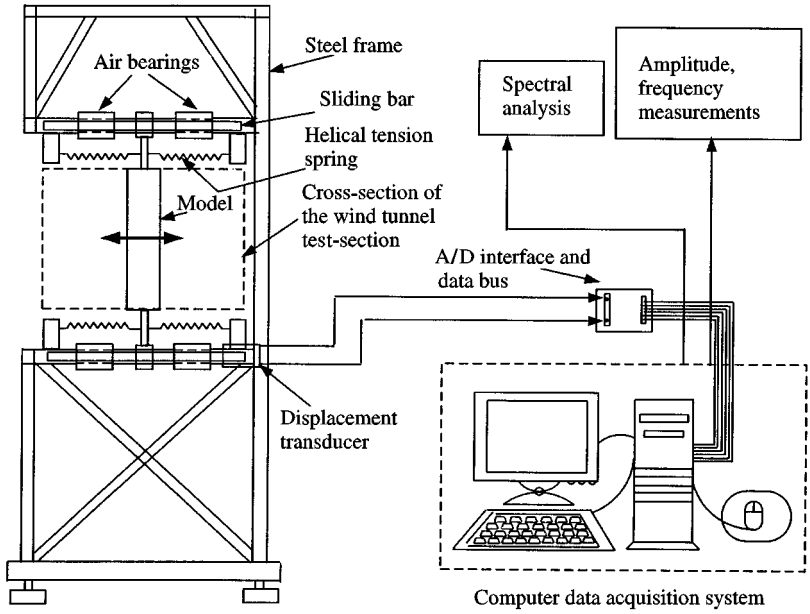

Figure 10. A schematic diagram of the dynamic experiment set-up involving the wind tunnel, test rig and data-acquisition system.

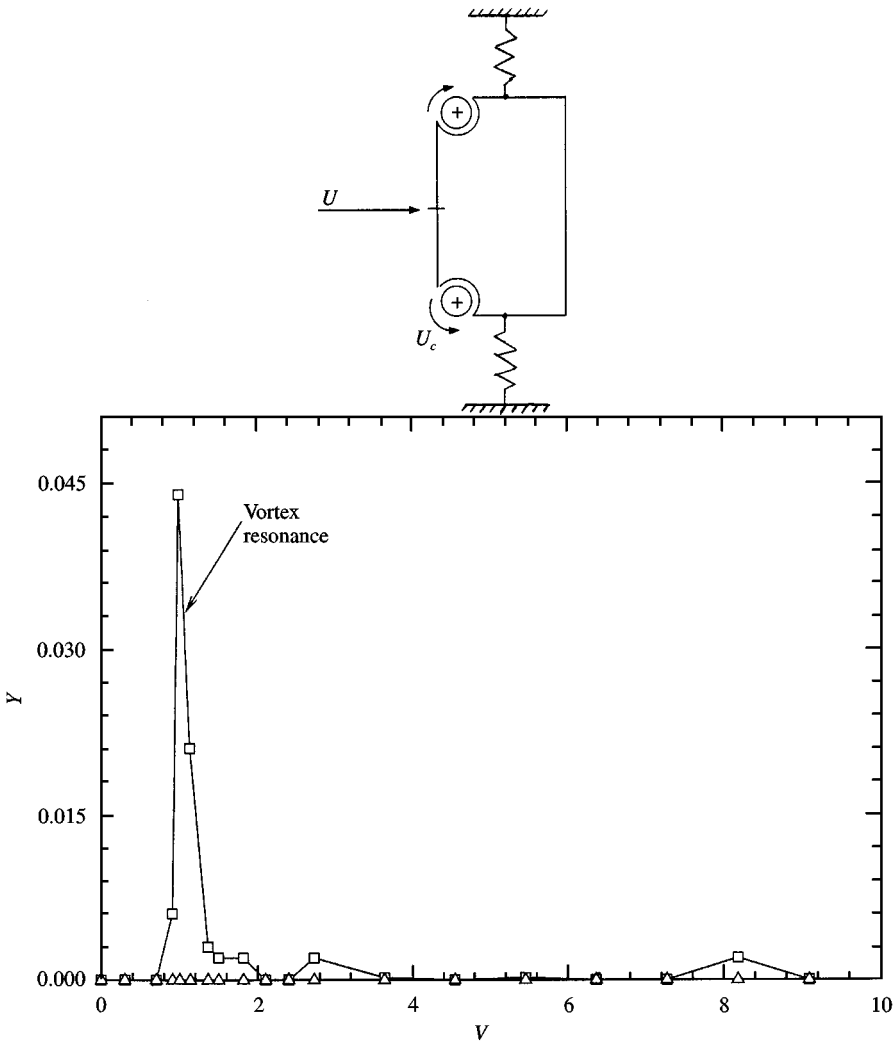

Figure 11. Effect of momentum injection on the galloping instability of a rectangular prism (AR = 0.5) at $\alpha = 0$, $\beta = 0.002693$: –□–, $U_c/U = 0$; Δ, $U_c/U = 1$. Note, the prism experiences vortex resonance, but is stable in galloping.

instability. At the momentum injection corresponding to $U_c/U = 1$, the rectangular prism does not exhibit either vortex resonance or galloping. The stability of the prism is restored completely. This is in accord with the prediction based on the simple stability criterion mentioned earlier. It is remarkable that, despite completely different mechanisms responsible for vortex resonance and galloping type of instabilities, the momentum injection is effective in suppressing both of them.

3. FLOW VISUALIZATION

To get a better appreciation as to the physical character of the complex flow field as affected by the angle of attack and momentum injection parameters, an extensive flow visualization

study was undertaken. This also gave useful information about the relative importance of the various parameters, and hence assisted in planning of the experiments as well analysis of the test data. The flow visualization tests were carried out in a closed-circuit water-channel facility. The models were constructed from Plexiglas and fitted with rotating cylinders driven by variable speed d.c. motors. A suspension of fine polyvinyl chloride powder was used in conjunction with slit lighting to visualize streamlines. Both angle of attack and cylinder speed were systematically changed, and still photographs as well as video movies were taken. The Reynolds number was 23 400.

The results for the rectangular prism at $\alpha = 0$ are presented in Figures 12 and 13. In the absence of any momentum injection, the top and bottom faces are immersed in a separated flow field. A large vortex can be seen in the process of formation. A saddle-point type of instability associated with the newly formed vortex can be clearly seen in the flow visualization photograph and the associated sketch [Figure 12, $U_c/U = 4$; Figure 13(b)]. The wake vortex structure displayed considerable turbulence, with associated mixing and dissipation. The separating shear layer from the top has a sinusoidal character and divides the wake into well-defined pockets of diffused vorticity, generated from the viscous dissipation of shed vortices. The overall configuration of the wake reverses itself in an alternative manner in phase with the vortex-shedding process. The video revealed considerable unsteadiness of the wake, oscillating from side to side due to the low-pressure region associated with the nascent vortex. The shed vortices grow rapidly as they are convected downstream, diffusing vorticity in the surrounding fluid at a faster rate. As U_c/U is increased from zero, the wake

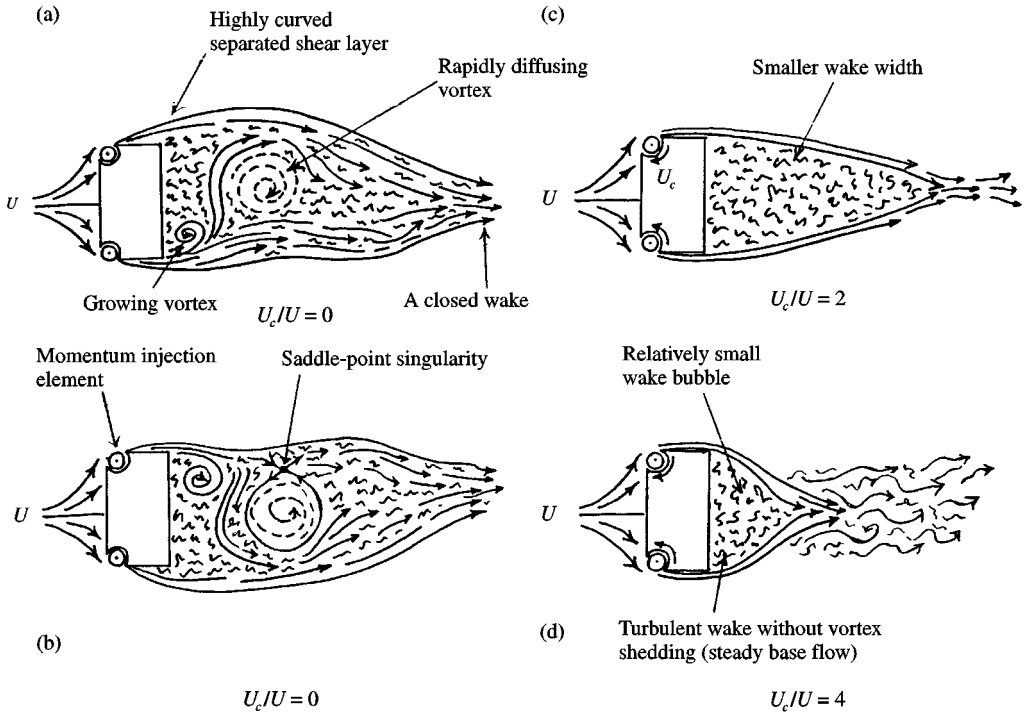

Figure 13. Effect of momentum injection on the characteristic features of the wake and the shed vortex system, as inferred from the flow visualization study.

gradually becomes narrower and the vortex formation is suppressed. Originally, unsteady flow in the wake ($U_c/U = 0$) turns into a steady separation bubble ($U_c/U = 4$). The near wake becomes a steady base flow region (Tanner 1975). There is an associated rise in the wake pressure which reduces the drag coefficient as seen before. Note, the stagnation point on the front face has moved away from the mid-point towards the bottom corner. The flow visualization study confirms, rather conclusively, the effectiveness of moving-surface boundary-layer control.

4. CONCLUDING REMARKS

Based on the static and dynamic wind-tunnel tests, theoretical prediction and flow visualization study, the following general comments can be made.

(i) Application of MSBC results in a significant rise in the wake pressure and suppression of vortex shedding. There is an associated reduction in the drag (average 36%), which is quite significant.

(ii) Extensive experiments over a range of the angle of attack and cylinder rotation suggest that, for most circumstances, a maximum momentum injection corresponding to $U_c/U = 3$ is sufficient to delay boundary-layer separation and achieve a minimum drag condition.

(iii) The results indicate the virtual elimination of vortex resonance and galloping type of instabilities in the presence of MSBC. The suppression of galloping is also predicted successfully from the quasisteady analysis.

(iv) The analysis based on the universal Strouhal number (Su) confirms the observation that the wakes of a bluff body at different orientations are similar, except for changes in the geometric and velocity scales.

(v) The flow visualization study provides qualitative insight into the character of the flow and confirms the effectiveness of MSBC as a versatile method for boundary-layer control.

(vi) The concept of MSBC offers exciting opportunities for drag reduction and vibration control of real-life structures.

ACKNOWLEDGMENT

The investigation reported here was supported by the National Sciences and Engineering Research Council of Canada, Grant No. A-2181.

References

Bearman, P. W. 1967 On vortex street wakes. *Journal of Fluid Mechanics* **28,** 625–641.

Bearman, P. W. 1984 Vortex shedding from oscillating bluff bodies. *Annual Review of Fluid Mechanics* **16**, 195–222.

Berger, E. & Wille, R. 1972 Periodic flow phenomena. *Annual Review of Fluid Mechanics* **4,** 313–340.

Den Hartog, J. P. 1985 *Mechanical Vibrations.* pp. 299–309. New York: Dover.

Hamel-Derouich 1991 Fluid loading on rectangular cylinders in steady flow. *Proceedings of First International Offshore and Polar Engineering Conference*, Vol. III, pp. 258–263, Edinburgh, U.K.

Hussaini, M. Y. & Salas, M. D. 1987 *Studies of Vortex Dominated Flows.* New York: Springer.

Kubo, Y., Hayashida, K., Kotsubo, C. & Kato, K. 1984 On the suppression of aerodynamic vibrations of a square prism in high angles of attack by boundary-layer control method. *First World Conference on Structural Control*, pp. TP1-13 to TP1-20, Los Angeles, U.S.A.

Li, Q. S. & Melbourne, W. H. 1995 Effects of turbulence on surface pressure of a flat plate and rectangular cylinders in separated and reattaching flows. *Proceedings of the Ninth International Conference on Wind Engineering*, pp. 165–176. New Delhi, India. New Delhi: Wiley Eastern Limited.

Mair, W. A. & Maull, D. J. 1971 Bluff bodies and vortex shedding — a report on Euromech 17. *Journal of Fluid Mechanics* **45,** 209–224.

Marris, A. W. 1964 A review on vortex streets, periodic wakes, and induced vibration phenomena. *ASME Journal of Basic Engineering* **86,** 185–196.

Modi, V. J., Mokhtarian, F., Fernando, M. S. U. K. & Yokomizo, T. 1991 Moving surface boundary-layer control as applied to two-dimensional airfoils. *Journal of Aircraft* **28,** 104–112.

Modi, V. J., Welt, F. & Seto, M. L. 1995 Control of wind induced instabilities through application of nutation dampers: a brief overview. *Journal of Engineering Structures* **17**, 626–638.

Munshi, S. R., Modi, V. J. & Yokomizo, T. 1995 Drag reduction and vibration suppression of a D-section structural member through momentum injection. *International Journal of Offshore and Polar Engineering* **5,** 161–165.

Nakamura, Y. 1993 Bluff-body aerodynamics and turbulence. *Journal of Wind Engineering and Industrial Aerodynamics* **49,** 65–78.

Nakamura, Y., Hirata, K. & Urabe, T. 1991 Galloping of rectangular cylinders: effects of downstream splitter plate. *Proceedings of International Conference on Flood Induced Vibrations*, Brighton, U.K. *Proceedings of I. Mech. E.*, Vol. 1991-6, Paper C416/046, pp 453–458. London: I. Mech. E.

Norberg, C. 1993 Flow around rectangular cylinders: pressure forces and wake frequencies. *Journal of Wind Engineering and Industrial Aerodynamics* **49,** 187–196.

Parkinson, G. V. & Brooks, N. P. H. 1961 On the aeroelastic instability of bluff cylinders. *Journal of Applied Mechanics* **28,** 252–258.

Parkinson, G. V. 1989 Phenomenon and modelling of flow-induced vibrations of bluff bodies. *Progress in Aerospace Science* **26,** 169–224.

Rosenhead, L. 1953 Vortex systems in wakes. *Advances in Applied Mechanics* **3,** 185–195.

Roshko, A. 1955 On the wake and drag of bluff bodies. *Journal of Aeronautical Sciences* **22,** 124–132.

Roshko, A. 1993 Perspectives on bluff body aerodynamics. *Journal of Wind Engineering and Industrial Aerodynamics* **49,** 79–100.

Tanner, M. 1975 Reduction of base drag. *Progress in Aerospace Science* **16,** 369–384.

Williamson, C. H. K. 1996 Vortex dynamics in the cylinder wake. *Annual Review of Fluid Mechanics* **28,** 447–539.

Zdravkovich, M. M. 1981 Review and classification of various aerodynamic and hydrodynamic means for suppressing vortex shedding. *Journal of Wind Engineering and Industrial Aerodynamics* **7,** 145–189.

APPENDIX: NOMENCLATURE

AR	aspect ratio (length to height ratio, H/D, for a bluff body)
C_D	sectional drag coefficient, $F_D/\frac{1}{2}\rho U^2 D$
C_L	sectional lift coefficient, $F_L/\frac{1}{2}\rho U^2 D$
C_y	lateral force coefficient, $-(C_L + C_D \tan\alpha)\sec\alpha$
C_P	pressure coefficient
C_{Pb}	base-pressure coefficient in the wake
$D = 2R$	frontal height of the rectangular prism
F_D, F_L	mean drag and lift forces, respectively
F_y	lateral force
$F(\alpha)$, $G(\alpha)$	functions depending on the angle of attack
H	length of the rectangular prism in freestream direction
I	work done over one cycle of galloping oscillations
L_x	turbulence length scale
P_i $(i = 1, 3, 5, 7)$	coefficients of polynomial expansion, equation (5)

R	characteristic radius of the bluff body, $D/2$
Re	Reynolds number, UD/v
S	circumferential length along the contour of the rectangular prism
St	Strouhal number, $f_v D/U$
St_p	Strouhal number based on the projected height normal to the flow, $f_v h/U$
Su	universal Strouhal number
U	freestream wind speed
U_c	cylinder surface speed
U_{cr}	critical cylinder surface speed for maximum drag reduction
U_c/U	momentum injection parameter
V	nondimensional wind speed, $U/(\omega_n D)$
V_c	critical wind speed for the onset of galloping oscillations
Y	nondimensional transverse amplitude, $y(\omega_n h)$
f	frequency, Hz
f_n	structure natural frequency
f_v	frequency of vortex shedding
h	projected height normal to the flow
k	stiffness
k_1	base pressure parameter, $\sqrt{1 - C_{Pb}}$
l_1	span of the bluff body
m	mass of the structure
n	mass parameter, $\frac{1}{2}\rho D^2 l_1/m$
r	system damping ratio
t	time
y	coordinate direction transverse to the freestream
$\dot{y}$, $\ddot{y}$	transverse velocity, $\mathrm{d}y/\mathrm{d}t$, and acceleration, $\mathrm{d}^2y/\mathrm{d}t^2$, respectively
α	angle of attack
β	nondimensional damping coefficient, $r/(2m\omega_n)$
v	kinematic viscosity of air
ρ	density of air
ω_n	circular natural frequency, $2\pi f_n$

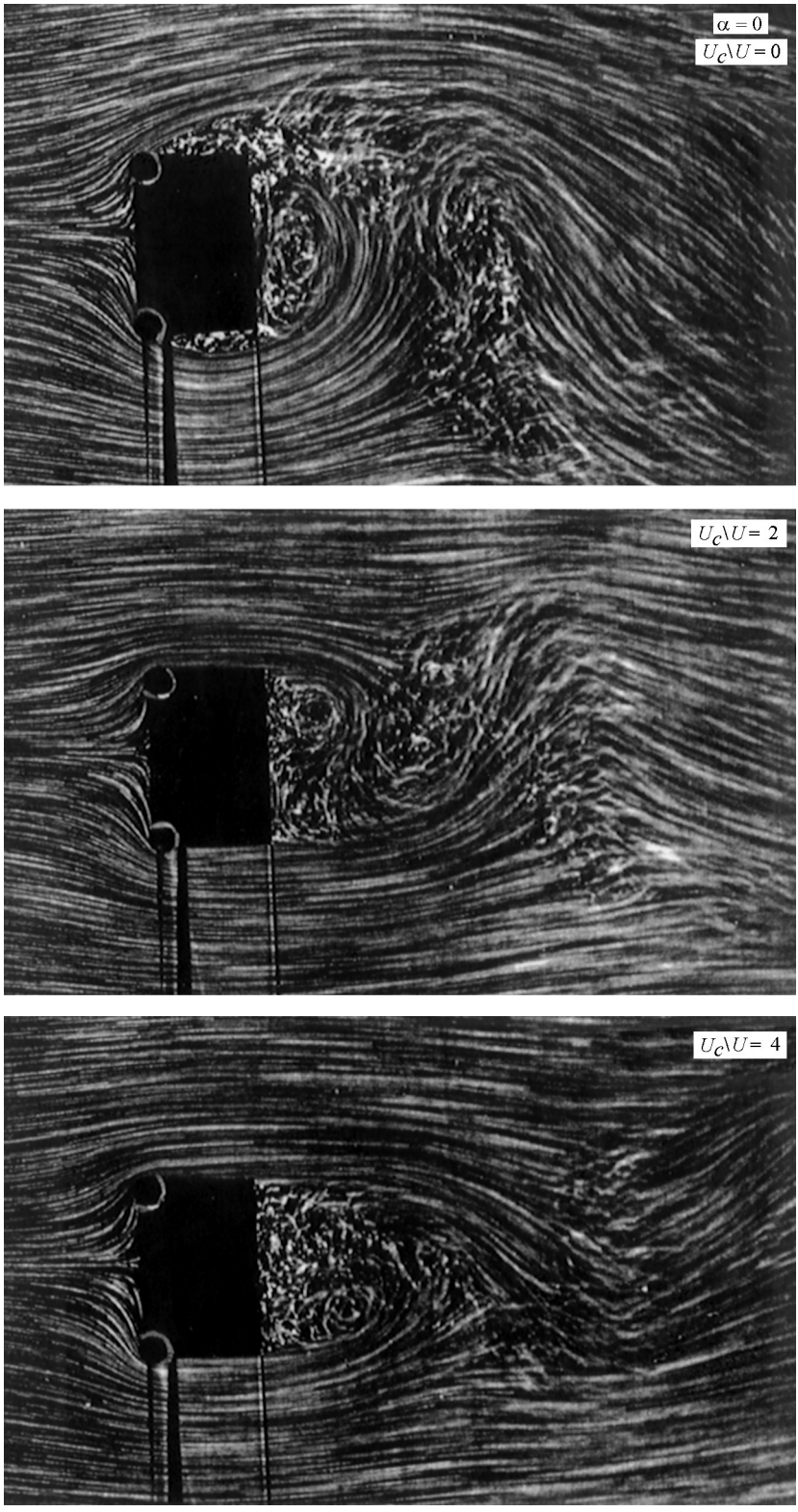

Figure 12. Effect of momentum injection on the characteristic features of the wake and the shed vortex system associated with the rectangular prism (AR = 0.5) as observed during the flow visualization study.